

Forbidden atomic oxygen emissions in the Martian dayside upper atmosphere

Susarla Raghuram^{a,*}, Sonal Kumar Jain^b and Anil Bhardwaj^a

^aPhysical Research Laboratory, Ahmedabad, 380009, India.

^bLaboratory for Atmospheric and Space Physics, University of Colorado Boulder, Boulder, CO, USA.

ARTICLE INFO

Keywords:

Mars, Atmosphere
Abundances, atmospheres
Atmospheres, chemistry
Atmospheres, composition
Aeronomy

ABSTRACT

Recently, Nadir and Occultation for Mars Discovery (NOMAD) ultraviolet and visible spectrometer instrument on board the European Space Agency's ExoMars Trace Gas Orbiter (TGO) simultaneously measured the limb emission intensities for both [OI] 2972 and 5577 Å (green) emissions in the dayside of Martian upper atmosphere. But the atomic oxygen red-doublet emission lines ([OI] 6300 and 6364 Å), which are expected to be observed along with [OI] 5577 and 2972 Å emissions, are found to be absent in the NOMAD-TGO dayside observed spectra. We aim to explore the photochemistry of all these forbidden atomic oxygen emissions ([OI] 2972, 5577, 6300, 6464 Å) in the Martian daylight upper atmosphere and suitable conditions for the simultaneous detection of these emission lines in the dayside visible spectra. A photochemical model is developed to study the production and loss processes of O(¹S) and O(¹D), which are the respective excited states of green and red-doublet emissions, by incorporating various chemical reactions of different O-bearing species in the upper atmosphere of Mars. By reducing Fox (2004) modelled neutral density profiles by a factor of 2, the calculated limb intensity profiles for [OI] 5577 and 2972 Å emissions are found to be consistent with the NOMAD-TGO observations. In this case, at altitudes below 120 km, our modelled limb intensity for [OI] 6300 Å emission is smaller by a factor 2 to 5 compared to that of NOMAD-TGO observation for [OI] 2972 Å emission, and above this distance it is comparable with the upper limit of the observation. We studied various parameters which can influence the limb intensities of these atomic oxygen forbidden emission lines. Our calculated limb intensity for [OI] 6300 Å emission, when the Mars is at near perihelion and for solar maximum condition, suggests that all these forbidden emissions should be observable in the NOMAD-TGO visible spectra taken on the dayside of Martian upper atmosphere. More simultaneous observations of forbidden atomic oxygen emission lines will help to understand the photochemical processes of oxygen-bearing species in the dayside Martian upper atmosphere.

*Corresponding author

✉ raghuramsusarla@gmail.com (S. Raghuram)

ORCID(s): 0000-0002-1309-2499 (S. Raghuram); 0000-0002-1722-9392 (S.K. Jain); 0000-0003-1693-453X (A. Bhardwaj)

1. Introduction

Forbidden atomic oxygen emissions are the prominent features in the visible spectra of terrestrial atmospheres. These emissions have been studied extensively from various ground- and space-based observatories. Observation of these emissions provides valuable information about the energy deposition and chemical processes in the upper atmospheres of terrestrial planets. About 5% of excited atomic oxygen atoms produced in 1S state decay directly to the ground state (3P) and produce [OI] 2972 Å emission, and the rest decay via 1D state that results in the emission at wavelength 5577 Å (green line). Radiative decay of $O(^1D)$ to the ground state produces the red-doublet emissions at wavelengths 6300 and 6364 Å, provided it is not collisionally quenched by other species. Since both [OI] 2972 and 5577 Å emissions are produced due to de-excitation of same electronic excited state (1S), detection of one of these lines confirms the presence of other. Similarly, the observation of green line also indicates the presence of red-doublet emissions but the opposite is not always true in case the $O(^1S)$ state is not produced in the atmosphere or totally deactivated by collisions.

Several theoretical works were carried out to study the photochemistry of metastable atomic oxygen atoms in the Martian upper atmosphere. About 40 years ago, Fox and Dalgarno (1979) predicted the forbidden emissions of atomic oxygen in the upper atmosphere of Mars. Simon et al. (2009) developed a kinetic model to study the seasonal variation of the dayside [OI] 2972 Å emission intensity along with other important emissions, such as CO_2^+ UV-doublet and CO Cameron bands. These modelling studies show that photodissociative excitation of CO_2 is the major source of $O(^1S)$ in the upper atmosphere of Mars. But the study of these emissions by Huestis et al. (2010) shows that dissociative recombination of O_2^+ also plays an important role in producing $O(^1S)$ and determining the [OI] 2972 and 5577 Å emission intensities. Hence, it is suggested that the observed [OI] 2972 Å emission intensity should be used to monitor the Martian ionosphere and not the ambient neutral temperature. The calculations made by Gronoff et al. (2012a) and Gronoff et al. (2012b) showed that the uncertainties associated with modelling parameters can influence the calculated limb intensities of spectroscopic emissions. To understand the photochemistry of these forbidden emissions, Jain (2013) accounted for several production and loss mechanisms of $O(^1S)$ and $O(^1D)$ in the Martian upper atmosphere

and modelled the atomic oxygen emission intensities for both solar maximum and minimum conditions. Recently, Gkouvelis et al. (2018) have reported observations of [OI] 2972 Å emission in the Imaging Ultraviolet Spectrograph (IUVS) onboard Mars Atmosphere and Volatile Evolution (MAVEN) satellite observed ultraviolet spectra and constrained the quantum yield for photodissociation of CO_2 producing $O(^1S)$ at Ly- α wavelength (1216 Å) as about 8%.

The observation of [OI] 2972 Å emission has been done in the Martian upper atmosphere by several spacecraft-borne ultraviolet spectrometers starting from Mariner 6 to the recent MAVEN mission (Stewart, 1972; Leblanc et al., 2006; Jain et al., 2015). But the observation of [OI] 5577 Å emission had never been reported in the dayside of Martian upper atmosphere until the recent detection from Nadir and Occultation for Mars Discovery ultraviolet and visible spectrometer instrument on board the European Space Agency's ExoMars Trace Gas Orbiter (NOMAD-TGO) by Gérard et al. (2020). Owing to its wide detection range (2000–6500 Å), this spectrometer is capable of observing the four forbidden atomic oxygen emissions ([OI] 2972, 5577, 6300, and 6364 Å) simultaneously in the Martian upper atmosphere. NOMAD-TGO could observe both [OI] 2972 and 5577 Å emissions simultaneously and the observed intensity ratio is used to determine the corresponding transition probabilities ratio of $O(^1S)$. However, the emission features at [OI] red-doublet wavelengths were found to be absent in the NOMAD-TGO observed dayside spectra (at the 1σ level, Gérard et al., 2020). We aim to study the photochemistry of these forbidden emission lines in the dayside of Martian upper atmospheres and explore suitable conditions to observe all these emissions simultaneously in the NOMAD-TGO spectra. By accounting for the important production and loss mechanism of $O(^1S)$ and $O(^1D)$ in our well utilized photochemical model, we studied the emission processes of forbidden atomic oxygen emission lines in the dayside Martian upper atmosphere. The model inputs and calculations are presented in Section 2. We present the results of our model calculations and discussion in Section 3. In Section 4, this work is summarized and conclusions are drawn.

2. Model inputs and calculations

A detailed description of the model calculations is provided in our earlier work (Jain, 2013; Jain and Bhardwaj, 2012; Raghuram and Bhardwaj, 2012; Bhardwaj and Raghuram, 2012; Raghuram and Bhardwaj, 2020). Here we briefly

describe the model inputs that are used for the present calculations. The neutral density profiles for the primary species (CO_2 , CO , N_2 , O_2 , and O) of Martian upper atmosphere are considered from Fox (2004), which are based on the Viking measurements and for solar minimum condition. To compare these density profiles with the ongoing Neutral Gas and Ion Mass Spectrometer (NGIMS) on-board MAVEN mission measurements, we analysed NGIMS/MAVEN level 2 (L2), version 8, revision 1 data for the period April to December 2019, during which NOMAD-TGO measured the limb emission intensities of forbidden oxygen emission lines in the Martian upper atmosphere. More details of the L2 data product are available in Benna and Elrod (2018) and the data can be accessed from a web link (<https://pds-atmospheres.nmsu.edu>). We noticed that most of the NGIMS/MAVEN measurements from April to December 2019 were on the night side of the Mars. Due to the MAVEN being on the night side, we do not have NGIMS/MAVEN measured neutral atmospheric densities at the time of NOMAD-TGO dayside observations. During September 2019, observations were on the dayside Martian upper atmosphere for solar zenith angle (SZA) $<40^\circ$ and similar to the NOMAD-TGO observational conditions on 28 April 2019 (SZA = 30°) but at different Martian solar longitudes (L_s). We plotted neutral density profiles of Fox (2004) along with variability in the NGIMS/MAVEN measured CO_2 and O density profiles in Figure 1. The input solar radiation flux, which is a daily-averaged flux generated based upon on the Flare Irradiance Spectra Model-Mars (FISM-M) using the EUV calibrated band irradiance measured by Solar Extreme Ultraviolet Monitor (EUVM) instrument onboard MAVEN and interpolated Earth-based solar indices, in the wavelength region of 5–1900 Å is taken on 28 April 2019 (Eparvier et al., 2015; Thiemann et al., 2017, <https://pds-ppi.igpp.ucla.edu>). As a case study, we also calculated the limb intensity profiles for forbidden atomic oxygen emissions for solar maximum condition by considering the neutral atmospheric model from Fox (2004). For this calculation, we used EUVM onboard MAVEN measured solar flux on 12 December 2014 during which Mars was at perihelion.

The input photon and electron impact cross sections are described in Jain (2013). Here we considered the total absorption cross section of CO_2 and the yield for the photodissociative excitation of CO_2 producing $\text{O}(^1\text{S})$ from Gkouvelis et al. (2018). Based on the discussion of Gkouvelis et al. (2018), we have taken a quantum yield of 0.09 for the dis-

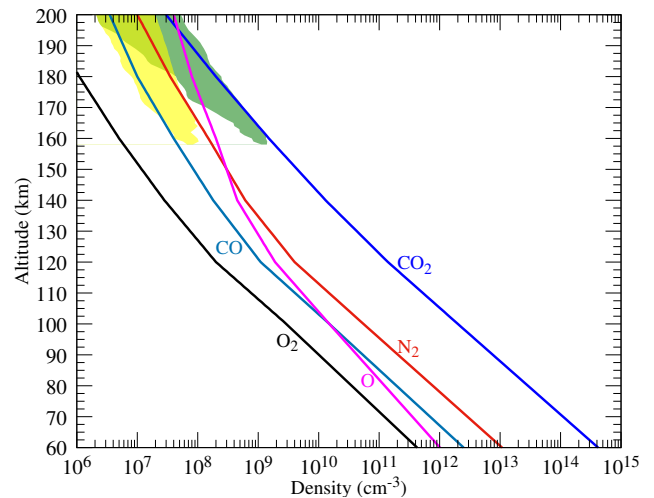


Figure 1: Neutral density distribution in the Martian upper atmosphere. The density profiles of major species are taken from Fox (2004) for solar minimum condition. Green and yellow shaded areas represent the variability in the NGIMS measured CO_2 and O densities during September 2019 for solar zenith angle less than 40° .

sociative recombination of O_2^+ producing $\text{O}(^1\text{S})$. Following the assumptions of Gkouvelis et al. (2018) and Jain (2013), we considered the quantum yields for the thermal recombination of CO_2^+ producing $\text{O}(^1\text{S})$ and $\text{O}(^1\text{D})$ as 0.05 and 0.59, respectively. However, we vary these assumed yields to study the impact of dissociative recombination of CO_2^+ on the modelled limb intensities. The photochemical reaction network used for calculating various production and loss rates of $\text{O}(^1\text{S})$ and $\text{O}(^1\text{D})$ is presented in Table 1. Electron and neutrals temperature profiles are taken from Fox and Hać (2009) for solar minimum and maximum conditions.

3. Results and Discussion

The modelled production rate and loss frequency profiles of $\text{O}(^1\text{S})$ and $\text{O}(^1\text{D})$ for various photochemical processes in the Martian upper atmosphere are presented in Figure 2. The calculated volume production rate profiles in Figure 2 (a) show that the total $\text{O}(^1\text{S})$ formation rate, which is majorly due to photodissociative excitation of CO_2 , has a double peak structure with lower and upper peaks at altitudes of 85 and 135 km, respectively. Photodissociative excitation of CO_2 by the solar radiation flux at HI Lyman- α wavelength causes the lower production peak, whereas the upper production peak is controlled by the flux mainly in wavelength region 860–1160 Å. The formation rate of $\text{O}(^1\text{S})$ due to other excitation mechanisms is smaller by a factor of 3 or more compared to that from photodissociative excitation of CO_2 .

Table 1Photochemical reactions for the formation and destruction of O(¹D) and O(¹S) in the Martian upper atmosphere

No.	Reaction	Rate Coefficient	Reference
R1	$h\nu + \text{CO}_2 \rightarrow \text{O}(\text{}^1\text{S}) + \text{CO}$	1.63×10^{-7}	This work
R2	$h\nu + \text{CO} \rightarrow \text{O}(\text{}^1\text{S}) + \text{C}$	1.43×10^{-8}	This work
R3	$h\nu + \text{O}_2 \rightarrow \text{O}(\text{}^1\text{S}) + \text{O}$	1.28×10^{-8}	This work
R4	$e_{ph} + \text{CO}_2 \rightarrow \text{O}(\text{}^1\text{S}) + \text{CO}$	Calculated	This work
R5	$e_{ph} + \text{CO} \rightarrow \text{O}(\text{}^1\text{S}) + \text{C}$	Calculated	This work
R6	$e_{ph} + \text{O}_2 \rightarrow \text{O}(\text{}^1\text{S}) + \text{O}$	Calculated	This work
R7	$e_{ph} + \text{O} \rightarrow \text{O}(\text{}^1\text{S}) + \text{O}$	Calculated	This work
R8	$\text{CO}_2^+ + e_{th} \rightarrow \text{O}(\text{}^1\text{S}) + \text{CO}$	$4.2 \times 10^{-7} (300/T_e)^{0.75}$	Viggiano et al. (2005)*
R9	$\text{O}_2^+ + e_{th} \rightarrow \text{O}(\text{}^1\text{S}) + \text{CO}$	$1.95 \times 10^{-7} (300/T_e)^{0.7}$	Gkouvelis et al. (2020) [‡]
R10	$h\nu + \text{CO}_2 \rightarrow \text{O}(\text{}^1\text{D}) + \text{CO}$	2.72×10^{-7}	This work
R11	$h\nu + \text{CO} \rightarrow \text{O}(\text{}^1\text{D}) + \text{C}$	1.43×10^{-8}	This work
R12	$h\nu + \text{O}_2 \rightarrow \text{O}(\text{}^1\text{D}) + \text{O}$	6.8×10^{-7}	This work
R13	$e_{ph} + \text{CO}_2 \rightarrow \text{O}(\text{}^1\text{D}) + \text{CO}$	Calculated	This work
R14	$e_{ph} + \text{CO} \rightarrow \text{O}(\text{}^1\text{D}) + \text{C}$	Calculated	This work
R15	$e_{ph} + \text{O}_2 \rightarrow \text{O}(\text{}^1\text{D}) + \text{O}$	Calculated	This work
R16	$e_{ph} + \text{O} \rightarrow \text{O}(\text{}^1\text{D}) + e$	Calculated	This work
R17	$\text{CO}_2^+ + e_{th} \rightarrow \text{O}(\text{}^1\text{D}) + \text{CO}$	$4.2 \times 10^{-7} (300/T_e)^{0.75}$	Viggiano et al. (2005) [†]
R18	$\text{CO}^+ + e_{th} \rightarrow \text{O}(\text{}^1\text{D}) + \text{CO}$	$2.5 \times 10^{-8} (300/T_e)^{0.55}$	Rosén et al. (1998)
R19	$\text{O}_2^+ + e_{th} \rightarrow \text{O}(\text{}^1\text{D}) + \text{O}$	$2.21 \times 10^{-7} (300/T_e)^{0.46}$	Guberman (1988)
R20	$\text{O}(\text{}^1\text{S}) + e_{th} \rightarrow \text{O}(\text{}^1\text{D}) + e_{th}$	8.5×10^{-9}	Berrington and Burke (1981)
R21	$\text{O}(\text{}^1\text{S}) + \text{CO}_2 \rightarrow \text{O}(\text{}^3\text{P}) + \text{CO}_2$	$3.21 \times 10^{-11} \exp(-1323/T_n)$	Capetanakis et al. (1993)
R22	$\text{O}(\text{}^1\text{S}) + \text{CO} \rightarrow \text{O}(\text{}^3\text{P}) + \text{CO}$	$7.4 \times 10^{-14} \exp(-957/T_n)$	Capetanakis et al. (1993)
R23	$\text{O}(\text{}^1\text{S}) + \text{O}_2 \rightarrow \text{O}(\text{}^3\text{P}) + \text{O}_2$	$2.32 \times 10^{-12} \exp(-812/T_n)$	Capetanakis et al. (1993)
R24	$\text{O}(\text{}^1\text{S}) + \text{N}_2 \rightarrow \text{O}(\text{}^3\text{P}) + \text{N}_2$	5×10^{-17}	Atkinson and Welge (1972)
R25	$\text{O}(\text{}^1\text{S}) + \text{O}(\text{}^3\text{P}) \rightarrow 2 \text{O}(\text{}^1\text{D})$	2×10^{-14}	Krauss and Neumann (1975)
R26	$\text{O}(\text{}^1\text{S}) + e_{th} \rightarrow \text{O}(\text{}^3\text{P}) + e_{th}$	$7.3 \times 10^{-13} T_e^{0.94}$	Berrington and Burke (1981)
R27	$\text{O}(\text{}^1\text{S}) \rightarrow \text{O}(\text{}^1\text{D}) + h\nu_{5577\text{Å}}$	1.26	Wiese et al. (1996)
R28	$\text{O}(\text{}^1\text{S}) \rightarrow \text{O}(\text{}^3\text{P}) + h\nu_{2972\text{Å}}$	0.075	Wiese et al. (1996)
R29	$\text{O}(\text{}^1\text{D}) + \text{CO}_2 \rightarrow \text{O}(\text{}^3\text{P}) + \text{CO}_2$	$6.8 \times 10^{-11} \exp(117/T_n)$	Streit et al. (1976)
R30	$\text{O}(\text{}^1\text{D}) + \text{N}_2 \rightarrow \text{O}(\text{}^3\text{P}) + \text{N}_2$	$1.8 \times 10^{-11} \exp(107/T_n)$	Atkinson et al. (1997)
R31	$\text{O}(\text{}^1\text{D}) + \text{CO} \rightarrow \text{O}(\text{}^3\text{P}) + \text{CO}$	1×10^{-11}	Schofield (1978)
R32	$\text{O}(\text{}^1\text{D}) + \text{O}_2 \rightarrow \text{O}(\text{}^3\text{P}) + \text{O}_2$	$3.2 \times 10^{-11} \exp(67/T_n)$	Atkinson et al. (1997)
R33	$\text{O}(\text{}^1\text{D}) + \text{O}(\text{}^3\text{P}) \rightarrow 2 \text{O}(\text{}^3\text{P})$	$2.13 \times 10^{-12} + 2.60 \times 10^{-13} T_n^{0.5} - 2.24 \times 10^{-15} T_n$	Yee et al. (1990)
R34	$\text{O}(\text{}^1\text{D}) \rightarrow \text{O}(\text{}^3\text{P}) + h\nu_{6300\text{Å}}$	6.478×10^{-3}	Froese Fischer and Tachiev (2004)
R35	$\text{O}(\text{}^1\text{D}) \rightarrow \text{O}(\text{}^3\text{P}) + h\nu_{6364\text{Å}}$	2.097×10^{-3}	Froese Fischer and Tachiev (2004)
R36	$\text{O}(\text{}^1\text{D}) + e_{th} \rightarrow \text{O}(\text{}^3\text{P}) + e_{th}$	$1.6 \times 10^{-12} T_e^{0.91}$	Berrington and Burke (1981)

The unattenuated photodissociative excitation frequencies for reactions R1, R2, R3, R10, R11, & R12 are calculated at heliocentric distance of 1.57 AU;* This value is multiplied by 0.05, see Gkouvelis et al. (2020); [†] This rate coefficient is multiplied with a factor 0.59, see Jain (2013) and the main text; [‡] This rate coefficient is multiplied by a factor 0.09, see Gkouvelis et al. (2020) for more details; $h\nu$, e_{ph} , e_{th} , T_e and T_n represent solar photon, photoelectron, thermal electron, electron and neutral temperatures, respectively.

Various modelled volume production rate profiles presented in Figure 2 (b) show that the total formation rate of O(¹D) is controlled by different excitation sources. The lower volume production peak of O(¹D) at altitude of 90 km is mainly due to the photodissociative excitation of CO₂, whereas the upper peak (at an altitude of 130 km) is controlled by photodissociative excitation of CO₂, dissociative recombination of O₂⁺, and radiative decay of O(¹S). Electron impact excitation of atomic oxygen and dissociative recombination of O₂⁺ contribute equally to the total O(¹D) formation at al-

titudes above 170 km. Four excitation sources, viz., photodissociative excitation of CO₂, radiative decay of O(¹S), electron impact on atomic oxygen, and dissociative recombination of O₂⁺ together produce more than 95% of total O(¹D) in the altitude range of 60 to 220 km, whereas the other excitation sources play a minor role in the O(¹D) formation. We also determined the relative contributions of these excitation sources to the total formation of O(¹D) and found that the photodissociative excitation of CO₂ and radiative decay of O(¹S) together produce about 50% of total O(¹D) in the

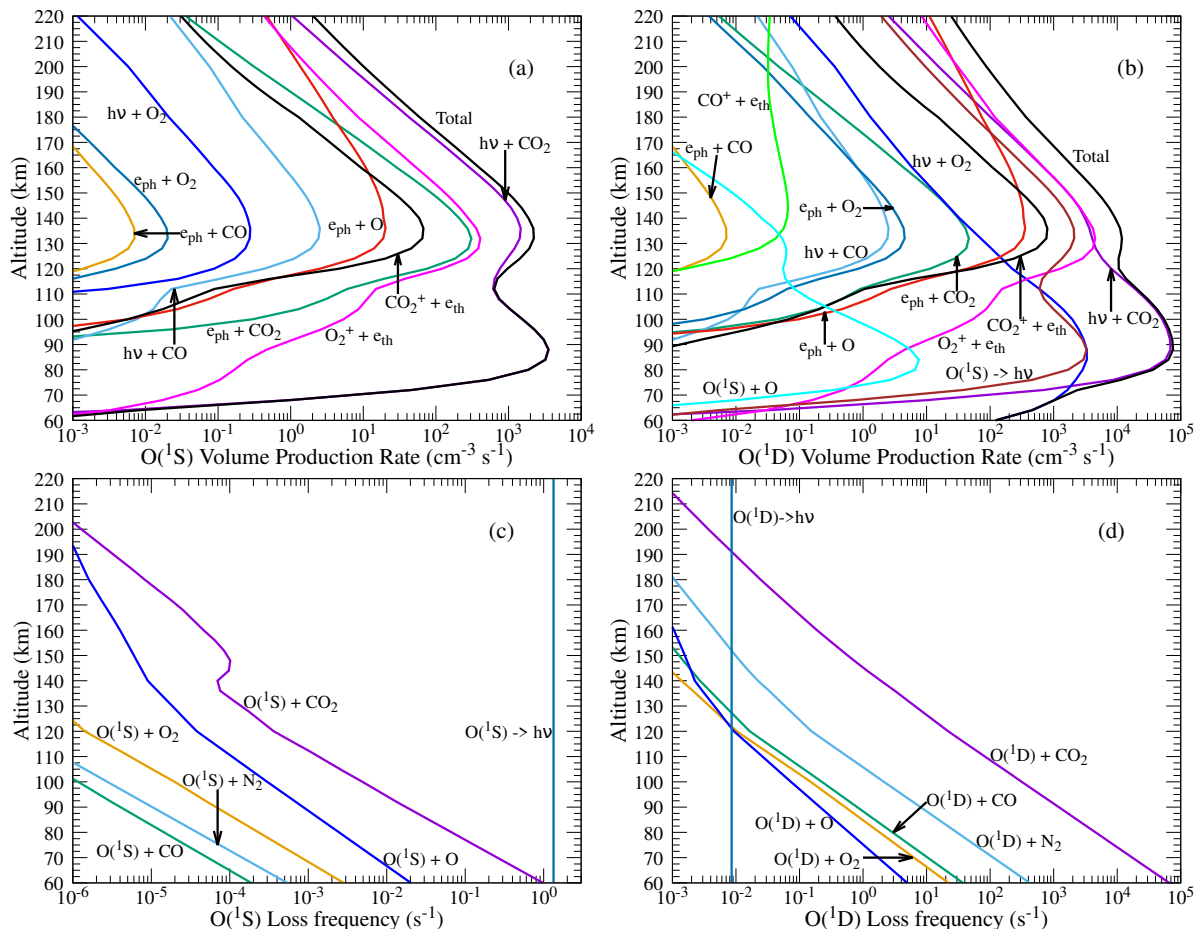


Figure 2: Modelled volume production rate (top panels) and loss frequency profiles (bottom panels) of $\text{O}(^1\text{S})$ and $\text{O}(^1\text{D})$ for different photochemical processes in the Martian upper atmosphere for solar zenith angle 30° using EUVM/MAVEN measured solar flux on 28 April 2019.

altitude range of 130 to 160 km and rest is majorly via electron impact on atomic oxygen and dissociative recombination of O_2^+ . Above 170 km altitude, the electron impact on atomic oxygen and dissociative recombination of O_2^+ gradually takes over as major production sources of $\text{O}(^1\text{D})$ (see Figure 2 (b)).

The modelled loss frequency profiles presented in Figure 2 (c) show that radiative decay is the dominant loss mechanism for $\text{O}(^1\text{S})$ in the Martian upper atmosphere. Owing to a short radiative lifetime (0.75 s), the collisional quenching with Martian neutral species has no impact on total loss frequency of $\text{O}(^1\text{S})$. As shown in Figure 2 (d), due to the long radiative lifetime (~ 120 s), the collisional quenching of $\text{O}(^1\text{D})$ by CO_2 is significant at altitudes up to 190 km, and above this distance radiative decay takes over as the dominant loss mechanism.

By incorporating the previously discussed different production and loss processes, the modelled density and volume

emission rate profiles for $\text{O}(^1\text{S})$ and $\text{O}(^1\text{D})$ are presented in Figure 3. The calculated density profile for $\text{O}(^1\text{S})$ has a double peak structure with respective upper and lower peaks at altitudes around 85 and 135 km (see solid green curve in Figure 3). These peaks are mainly due to the formation of $\text{O}(^1\text{S})$ via photodissociative excitation of CO_2 by solar radiation flux in different wavelength regions (see Figure 2 (a)). The modelled $\text{O}(^1\text{D})$ density profile has a broad peak in the altitude range of 150 to 200 km, which is determined by various production processes and the collisional quenching of $\text{O}(^1\text{D})$ by CO_2 (see solid red curve in Figure 3). This calculation shows that strong collisional quenching of $\text{O}(^1\text{D})$ substantially reduces its density at altitudes below 150 km. We calculated volume emission rates of these metastable species by multiplying the modelled density profiles with corresponding transition probabilities (see dashed curves in Figure 3). The radiative lifetime of $\text{O}(^1\text{S})$ is smaller by more than two orders of magnitude compared to that of $\text{O}(^1\text{D})$, which re-

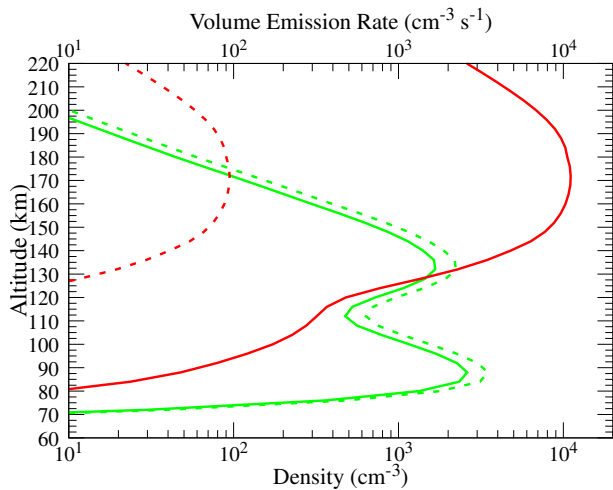


Figure 3: Modelled volume emission rate (dashed curves) and density (solid curves) profiles for $O(^1S)$ and $O(^1D)$ are plotted in the top and bottom x-axes, respectively. Green and red curves are the respective calculated profiles for $O(^1S)$ and $O(^1D)$.

sults in faster spontaneous decay compared to that of $O(^1D)$. Our modelled volume emission rates profiles show that radiative decay of $O(^1D)$ and $O(^1S)$ produce corresponding forbidden oxygen emissions with maximum intensities at altitudes above and below 140 km in the Martian upper atmosphere, respectively.

A comparison between the modelled limb emission intensity profiles and NOMAD-TGO observations for $[OI]$ 2972 and 5577 Å emissions is presented in Figure 4. By decreasing the neutral density profiles of Fox (2004) model by a factor of 2, which we call a standard case, the calculated limb emission intensity profiles for $[OI]$ 2972 and 5577 Å emissions are found to be consistent with NOMAD-TGO observations at altitudes below 150 km (see solid blue and green curves in Figure 4). This agreement suggests that photodissociative excitation of CO_2 is sufficient to explain the NOMAD-TGO observed limb intensities for $[OI]$ 2972 and 5577 Å emissions. At altitudes above 140 km, our modelled limb intensities are decreasing rapidly and smaller by an order of magnitude compared to NOMAD-TGO observation. However, it should be noted that the uncertainties in the NOMAD-TGO measured limb intensities for $[OI]$ 2972 and 5577 Å emissions are larger at altitudes above 140 km compared to those at lower altitudes.

We have considered Fox (2004) modelled neutral density profiles, which are based on the Viking measurements and for solar minimum condition, to calculate the limb intensities of forbidden atomic oxygen emission lines. As shown in Fig-

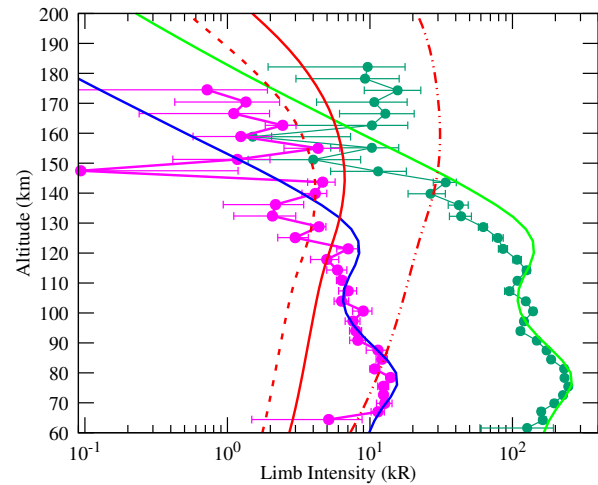


Figure 4: Comparison between modelled and observed limb intensity profiles of $[OI]$ 2972, 5577, and 6300 Å emissions. Magenta and thick green curves with x-error bars represent the respective NOMAD-TGO observed limb intensity profiles for $[OI]$ 2972 and 5577 Å emissions on 28 April 2019 (taken from Gérard et al., 2020). Blue, green and red curves are the modelled limb intensity profiles for $[OI]$ 2972, 5577 and 6300 Å emissions, respectively. These limb intensities are calculated by decreasing the Fox (2004) modelled neutral density profiles for solar minimum condition by a factor of 2. Dashed and dash double-dotted red curves represent the calculated limb intensity profiles for $[OI]$ 6300 Å emission by reducing the Fox (2004) modelled atomic oxygen density by a factor of 10 and for solar maximum condition, respectively.

ure 1, the in-situ measured CO_2 and O densities vary about an order of magnitude at altitudes around 200 km. Considering this variability into account, a reduction in the neutral density of Fox (2004) model by a factor of 2 is necessary to explain the observed limb intensity profiles. We compared the Fox (2004) neutral density profiles for solar minimum condition with Mars Climate Database (MCD) modelled neutral densities for NOMAD-TGO observational condition and found that they are nearly consistent. By reducing the neutral density profiles of MCD by a factor of 2, Gérard et al. (2020) also explained the observed emission limb intensity profiles of $[OI]$ 2972 and 5577 Å emissions. Our calculations and Gérard et al. (2020) study showed that the observed limb intensity profiles of forbidden oxygen emission (5577 & 2972 Å) lines can be used to constrain the neutral abundances, particularly CO_2 , in the Martian upper atmosphere.

For our standard case, the modelled intensity profiles of $[OI]$ 5577 and 6300 Å emissions via major production processes are presented in Figure 5. The calculated limb intensity profiles in the left panel of this figure show that most

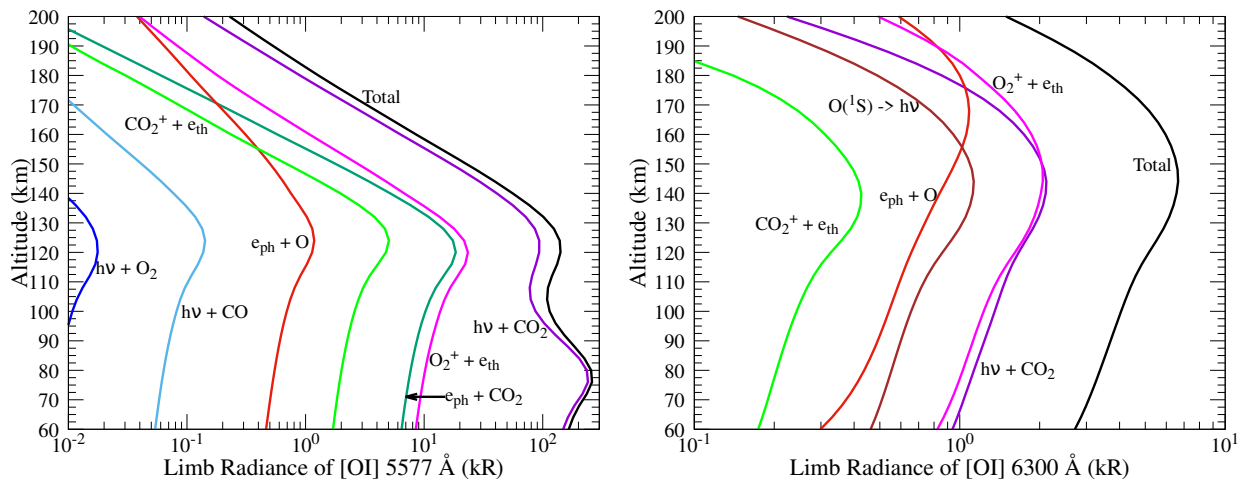


Figure 5: Modelled limb intensity profiles of [OI] 5577 Å (left panel) and 6300 Å (right panel) emissions for major formation processes in the Martian upper atmosphere.

of the [OI] 5577 Å emission produces via photodissociative excitation of CO_2 in the limb viewing geometry with a contribution more than 80% in the altitude range 60 to 200 km. The remaining significant contributions are from the thermal recombination of O_2^+ and electron impact excitation of atomic oxygen and CO_2 . Thus, the observed limb intensity of this emission can be used to constrain the CO_2 density in the upper atmosphere of Mars.

In the case of [OI] 6300 Å emission, for the altitudes below 170 km, we determined that the total limb intensity is controlled by photodissociation of CO_2 , thermal recombination of O_2^+ , electron impact on atomic oxygen, and radiative decay of $\text{O}(^1\text{S})$, with a relative contribution of about 35%, 30%, 10% and 15%, respectively (see the right panel of Figure 5). The remaining 10% of emission intensity is determined by several excitation sources as shown in Figure 2 (b). It can be noticed in this figure that above 170 km altitude, electron impact on atomic oxygen and thermal recombination of O_2^+ significantly contribute to the total limb intensity of [OI] 6300 Å emission. In the following section we discuss the role of various parameters which can influence the observed [OI] red-doublet limb intensities in the Martian upper atmosphere.

3.1. Effect of input parameters on the modelled red-doublet limb intensities

The branching ratios for $\text{O}(^1\text{D})$ radiative decay transitions show that the emission intensity of [OI] 6364 Å line should be about one third that of [OI] 6300 Å (see emission rates for reactions R34 and R35 in Table 1 and Wiese

et al., 1996). Hence, we present the calculated limb intensity profile only for [OI] 6300 Å emission and compare its magnitude with those of [OI] 2972 and 5577 Å emissions in Figure 4 (see red curves in this Figure).

The modelled limb intensity profile for [OI] 6300 Å emission, which is calculated for our standard case, has a broad peak in the altitude range of 120 to 170 km and comparable with the upper limit of [OI] 2972 Å observation (see solid red curve in Figure 4). At altitudes below 120 km, the modelled limb intensity of [OI] 6300 Å emission is smaller by a factor of 2 to 5 compared to that of NOMAD-TGO observation for [OI] 2972 Å emission (see solid red and magenta curves in Figure 4). This calculation shows that the modelled limb intensity for [OI] 6300 Å emission is significant compared to that of [OI] 2972 Å and should be observable in NOMAG-TGO dayside spectra taken in the altitude region of 120 to 170 km, provided sufficient signal-to-noise ratio in the measurement during the observation period.

As pointed out by Huestis and Slanger (2006), the photodissociative cross section of CO_2 producing $\text{O}(^1\text{D})$ was not experimentally determined before. But there are several recent developments in measuring the cross section for this excitation processes (Sutradhar et al., 2017; Lu et al., 2015; Song et al., 2014; Gao and Ng, 2019). However, these measured cross sections are limited to a small wavelength range from threshold to 1000 Å. Recently, Raghuram et al. (2020) modelled atomic oxygen green and red-doublet emissions in CO-dominated and water-poor comet C/2016 R2 (Pan-STARRS). By accounting for various photochemical processes, it was found that both green and red-doublet atomic

oxygen emissions are controlled by photodissociative excitation of CO_2 in the cometary coma of this comet. They also showed that the uncertainties associated with the photon cross section of CO_2 producing $\text{O}(^1\text{D})$ play an important role in determining the observed atomic oxygen green to red-doublet emission intensity ratio in comet C/2016 R2 (Pan-STARRS). By comparing the modelled and observed atomic oxygen green to red-doublet emission intensity ratios, Raghuram et al. (2020) suggested that the photodissociative excitation cross section of CO_2 producing $\text{O}(^1\text{D})$ should be increased by a factor of 3. Considering the uncertainty associated with this excitation process, when we increase the cross section for photodissociative excitation of CO_2 by a factor of 3, the modelled total [OI] 6300 Å limb intensity is found to be 60% higher compared to that of our standard case. This calculation suggests that the role of uncertainty associated with photodissociative excitation of CO_2 lead to higher [OI] red-doublet limb intensities than our standard case.

Due to lack of experimentally determined value, following the assumption of Jain (2013), we incorporated branching ratio for dissociative recombination of CO_2^+ producing $\text{O}(^1\text{D})$ as 0.59. Our calculations in Figure 2 (b) show that the dissociative recombination of CO_2^+ plays a minor role in the total production of $\text{O}(^1\text{D})$. Even with the assumed higher branching ratio, we find that this excitation process contributes little (<10%) to the total formation of $\text{O}(^1\text{D})$ when compared to that from other excitation sources in the Martian upper atmosphere. Hence, our assumed branching ratio has no impact on the modelled [OI] red-doublet limb intensities. Similarly, considering branching ratio from Gkouvelis et al. (2018) for dissociative recombination of CO_2^+ , our modelled production rate of $\text{O}(^1\text{S})$ is smaller by an order of magnitude or more compared to that from photodissociation of CO_2 . Thus, the assumed branching ratio for dissociative recombination of CO_2^+ has no impact on the modelled [OI] 2972 and 5577 Å limb intensities.

Collisional quenching of $\text{O}(^1\text{D})$ has an important role in determining the limb intensities of [OI] red-doublet emissions in the Martian upper atmosphere. By comparing the modelled total production rate and loss frequency profiles in Figure 2 we can understand that though $\text{O}(^1\text{D})$ is produced a by an order magnitude higher than that of $\text{O}(^1\text{S})$ for the altitudes below 140 km, the strong collisional quenching by CO_2 substantially reduces its density at lower altitudes (see Figure 3). We evaluated that about 30% of the total $\text{O}(^1\text{D})$

production is due to photodissociative excitation of CO_2 at altitudes above 140 km, and remaining is due to other excitation sources. Hence, larger amount of CO_2 significantly leads to strong collisional quenching of $\text{O}(^1\text{D})$ rather than its production. But it should be noted that the large amount CO_2 density in the Martian upper atmosphere also leads to an increase in the [OI] 2972 and 5577 Å limb emission intensities. The compilation of various experimentally determined $\text{O}(^1\text{D})$ quenching rates by Burkholder et al. (2015) and recent measurements by Nuñez-Reyes and Hickson (2018) showed that the uncertainty in measuring the rate coefficient of collisional reaction between CO_2 and $\text{O}(^1\text{D})$ is only about 20%, which suggests that larger quenching of $\text{O}(^1\text{D})$ in the Martian upper atmosphere is unlikely.

As discussed earlier, at altitudes above 170 km, the contribution from dissociative recombination of O_2^+ and electron impact excitation of atomic oxygen is significant to the total formation of $\text{O}(^1\text{D})$ (see Figure 2 and also the right panel of Figure 5). The formation of O_2^+ ion is mainly due the collisions between CO_2^+ and atomic oxygen. Hence, the change in neutral density profile of atomic oxygen can influence O_2^+ ion density and also total volume production of $\text{O}(^1\text{D})$ in the Martian upper atmosphere. As shown in Figure 1, the NGIMS/MAVEN measured atomic oxygen and CO_2 densities during September 2019 are varying by an order of magnitude at altitudes above 170 km. Using NGIMS/MAVEN measurements, we find that the measured volume mixing ratios of O/CO_2 are smaller by a factor of 2 to 10 compared to that of Fox (2004) in the altitude range of 150 to 200 km. Considering the variability in NGIMS/MAVEN measured densities into account, we decreased the Fox (2004) atomic oxygen density by an order of magnitude to study its impact on the modelled [OI] 6300 Å limb intensity. By decreasing the atomic oxygen density, we found that the modelled [OI] 6300 Å limb intensity is smaller by maximum factor of 2 compared to our standard case (see dashed red-curve in Figure 4). In this case, the contributions from both electron impact on atomic oxygen and thermal recombination of O_2^+ to the total $\text{O}(^1\text{D})$ production significantly decrease in the altitude range 60 to 200 km, whereas the radiative decay of $\text{O}(^1\text{S})$ and photodissociation of CO_2 majorly produce $\text{O}(^1\text{D})$ and cause the [OI] red-doublet emissions (see the right panel of Figure 5). This calculation shows that the variation in atomic oxygen density in the Martian upper atmosphere can lead to a significant change in the observed limb intensities of [OI] red-doublet emissions.

The NGIMS/MAVEN measurements in the altitude range of 150 to 200 km shows that the CO_2 and O densities can vary by an order magnitude and are also smaller than those of Fox (2004) model (see Figure 1). When we scaled the neutral densities of Fox (2004) model to the lower limit of NGIMS/MAVEN measurements, the calculated limb intensity for [OI] 6300 Å is closer to our standard case at altitudes below 120 km. This calculation shows that in spite of lower neutral densities than those of Fox (2004), the observed [OI] 6300 Å is not expected to change significantly compared to our standard case at altitudes below 120 km. Thus, the modelled limb intensity profile of [OI] 6300 Å for our standard case serves as an upper limit during NOMAD-TGO observation period.

The thermal structure of Martian upper atmosphere also plays an important role in determining the neutral densities and subsequently the emission intensities of forbidden atomic oxygen emission lines. During solar active condition, the densities of atomic oxygen and CO_2 increase in the upper atmosphere of Mars. We noticed in our calculations that the larger volume mixing ratio of atomic oxygen leads to higher limb intensities of [OI] 2972 and 5577 Å emissions only for altitudes above 150 km. But when we increase the atomic oxygen density in the model, the calculated limb intensity for [OI] 6300 Å emission also increased in the altitude range of 60 to 200 km. Hence, for higher thermospheric temperature all these emission lines are expected to be observed in the NOMAD-TGO dayside spectra. However, it should be noted that the NOMAD-TGO observations were carried out on Mars for solar longitudes between 16° and 115° when it was crossing the aphelion and the solar activity during this period was also low. Thus, larger neutral densities are not expected in the Martian upper atmosphere during NOMAD-TGO observation period.

During the NOMAD-TGO observation period, the background intensity level around wavelength 6300 Å is equivalent to more than 10 kR. Moreover, the [OI] red-doublet emission lines are closer to the longer wavelength limit of the NOMAD-TGO instrument and the detector has a reduced sensitivity in this region, which is the main reason for the absence of these emissions in the observed dayside spectra (personal communication, Gérard et al., 2020). Furthermore, most of the NOMAD-TGO observations took place when Mars was moving away from the Sun. But when Mars reaches perihelion, due to proximity of the Sun, the neutral densities of Martian upper atmosphere increases due to large

thermospheric temperature. We evaluated the limb intensity of [OI] 6300 Å emission during high solar activity and when Mars is at perihelion. For this case, we accounted for neutral atmosphere from Fox (2004) for solar maximum condition and used the EUVM/MAVEN measured solar flux on 12 December 2014 (during which Mars was at perihelion and solar activity was also high, $F_{10.7} = 152 \times 10^{-22} \text{ W m}^{-2} \text{ Hz}^{-1}$). We find that the modelled limb intensity [OI] 6300 Å emission is higher by a more than a factor of 3 than our standard case (see dash double-dotted red curve in Figure 4). In this case, the modelled [OI] 6300 Å peak emission limb intensity is about 30 kR at altitudes above 140 km and this emission line would have been seen in NOMAD-TGO spectra, provided that the background intensity is smaller compared to the modelled limb emission intensity. Thus, we suggest that the simultaneous detection of [OI] red-doublet emission along with other atomic forbidden emissions on the dayside Martian upper atmosphere by NOMAD-TGO would be possible when Mars is at perihelion.

Our calculations showed that there are a few parameters which determine the limb intensities of [OI] red-doublet emissions in the Martian upper atmosphere. In spite of variability in the neutral densities in the Martian upper atmosphere, we find that the modelled limb intensity of [OI] 6300 Å emission should be smaller than that of [OI] 2972 Å emission by a factor of 2 to 5 at altitudes below 120 km and it is higher above this altitude (see Figure 4). NOMAD-TGO should be able to detect these emissions in the dayside spectra provided sufficient signal-to-noise ratio during the observation. Instrument sensitivity coupled with uncertainties in the neutral atmosphere (given the large variability in atomic oxygen and CO_2 as shown Figure 1) may explain the absence of [OI] red-doublet emission lines in the dayside spectra taken during NOMAD-TGO observation period. However, when Mars gets closer to the Sun, the seasonal and solar cycle variations significantly affect the neutral densities of Martian upper atmosphere and result in the [OI] 6300 Å limb emission intensity within the observation limit of NOMAD-TGO. More simultaneous observations of forbidden atomic oxygen emissions are required to study the photochemistry of these emissions in the Martian upper atmosphere.

4. Summary and Conclusions

Recently, Nadir and Occultation for Mars Discovery ultraviolet and visible spectrometer instrument on board the European Space Agency's ExoMars Trace Gas Orbiter made

simultaneous detection of forbidden atomic oxygen emissions at wavelengths 2972 and 5577 Å in the spectra observed between 24 April and 1 December 2019 on the dayside Martian upper atmosphere. Thanks to the wide detection wavelength range of this instrument, it can measure the limb emission intensities of four forbidden atomic oxygen emissions at wavelengths 2972, 5577, 6300, and 6364 Å simultaneously. Since both [OI] 2972 and 5577 Å emissions originate from the same excited state of atomic oxygen, detection of any one of these emissions confirms the presence of other. Similarly, detection of [OI] 5577 Å emission line also indicates the presence of [OI] red-doublet emissions at wavelengths 6300 and 6364 Å, but the opposite is not true. However, these [OI] red-doublet emissions were not observed in the visible spectra taken during the NOMAD-TGO observation period due to the reduced sensitivity of the detector. By accounting for the important chemical pathways of $O(^1S)$ and $O(^1D)$, which are the excited states of these forbidden atomic oxygen emissions, we developed a model to study the photochemistry of these forbidden emissions in the Martian upper atmosphere and aimed to explore the suitable conditions to observe [OI] red-doublet emissions along with other atomic oxygen forbidden emissions. Our calculations show that NOMAD-TGO observed limb intensities for [OI] 2972 and 5577 Å emissions are mainly controlled by photodissociative excitation of CO_2 . On reducing neutral density profiles of Fox (2004) model for solar minimum condition by a factor of 2, our modelled limb intensities of [OI] 2972 and 5577 Å emissions are found to be in agreement with NOMAD-TGO observations.

We studied the role of different parameters which can influence the observation of [OI] red-doublet emissions in the dayside Martian upper atmosphere. The limb emission intensities of these emissions are found to be controlled by photodissociative excitation of CO_2 , radiative decay of $O(^1S)$, dissociative recombination of O_2^+ , and electron impact on atomic oxygen. Our modelled limb intensity profile of [OI] 6300 Å emission is comparable and higher than that of NOMAD-TGO observation for [OI] 2972 Å emission in the altitude range of 60 to 200 km. We find that the peak limb emission intensity for [OI] 6300 Å emission occurs at altitudes above 120 km and higher than the upper limit of NOMAD-TGO observation for [OI] 2972 Å emission. But at altitudes below 120 km, the modelled limb intensity for [OI] 6300 Å emission is smaller by a factor of 2 to 5 compared to that of NOMAD-TGO observation for [OI] 2972 Å emission.

Hence, [OI] 6300 Å emission line is expected to be observed in the dayside spectra of NOMAD-TGO at altitudes above 140 km provided that the signal-to-noise ratio is sufficient during the observation period. Due to the reduced detector sensitivity around the wavelength 6300 Å, NOMAD-TGO could not observe the [OI] red-doublet emission lines in the dayside of Mars. Moreover, most of the NOMAD-TGO observations took place when the Mars was travelling away from the Sun (L_s is varying from 16° to 115°), during which the neutral densities in the Martian upper atmosphere are smaller compared to those at near perihelion. Based on our modelling we suggest that all these atomic forbidden emissions should be observable in the dayside NOMAD-TGO spectra taken over the southern hemisphere, when Mars is at perihelion. More simultaneous observations of forbidden atomic oxygen emission lines are required to study the photochemistry of Martian upper atmosphere.

Acknowledgements

SR is supported by Department of Science and Technology (DST) with Innovation in Science Pursuit for Inspired Research (INSPIRE) faculty award [grant : dst/inspire/04/2016/002687], and he would like to thank Physical Research Laboratory for facilitating conducive research environment. Authors would like to thank the anonymous reviewers for their constructive comments and suggestions that improved this manuscript.

Data Availability

This paper make use of NGIMS/MAVEN measured neutral and ion number densities L2 data which has been accessed through the web link (<https://pds-atmospheres.nmsu.edu>) The modelled data in this research will be shared on reasonable request to the corresponding author.

References

- Atkinson, R., Baulch, D.L., Cox, R.A., Hampson, Jr., R.F., Kerr, J.A., Rossi, M.J., Troe, J., 1997. Evaluated Kinetic and Photochemical Data for Atmospheric Chemistry: Supplement VI. IUPAC Subcommittee on Gas Kinetic Data Evaluation for Atmospheric Chemistry. *Journal of Physical and Chemical Reference Data* 26, 1329–1499. doi:10.1063/1.556010.
- Atkinson, R., Welge, K.H., 1972. Temperature Dependence of $O(^1S)$ Deactivation by CO_2 , O_2 , N_2 , and Ar. *J. Chem. Phys.* 57, 3689–3693. doi:10.1063/1.1678829.
- Benna, M., Elrod, M., 2018. Mars atmosphere and volatile evolution (MAVEN) mission, neutral gas and ion mass spectrometer (NGIMS). NGIMS PDS Software Interface Specification, Revision 1.9 .

- Berrington, K.A., Burke, P.G., 1981. Effective collision strengths for forbidden transitions in e-N and e-O scattering. *Planetary and Space Science* 29, 377 – 381. doi:10.1016/0032-0633(81)90026-X.
- Bhardwaj, A., Raghuram, S., 2012. A coupled chemistry-emission model for atomic oxygen green and red-doublet emissions in the comet C/1996 B2 Hyakutake. *??jnlApJ* 748, 13. doi:10.1088/0004-637X/748/1/13.
- Burkholder, J.B., Sander, S.P., Abbatt, J., Barker, J.R., Huie, R.E., Kolb, C.E., Kurylo, M.J., Orkin, V.L., Wilmouth, D.M., Wine, P.H., 2015. Chemical kinetics and photochemical data for use in atmospheric studies, evaluation no. 18.
- Capetanakis, F.P., Sondermann, F., Höser, S., Stuhl, F., 1993. Temperature dependence of the quenching of O(¹S) by simple inorganic molecules. *??jnlJ. Chem. Phys.* 98, 7883. doi:10.1063/1.464596.
- Eparvier, F.G., Chamberlin, P.C., Woods, T.N., Thiemann, E.M.B., 2015. The Solar Extreme Ultraviolet Monitor for MAVEN. *??jnlSpace Sci. Rev.* 195, 293–301. doi:10.1007/s11214-015-0195-2.
- Fox, J.L., 2004. Response of the Martian thermosphere/ionosphere to enhanced fluxes of solar soft X rays. *J. Geophys. Res. (Space Physics)* 109, A11310. doi:10.1029/2004JA010380.
- Fox, J.L., Dalgarno, A., 1979. Ionization, luminosity, and heating of the upper atmosphere of Mars. *??jnlJ. Geophys. Res.* 84, 7315 – 7333. doi:10.1029/JA084iA12p07315.
- Fox, J.L., Hać, A.B., 2009. Photochemical escape of oxygen from Mars: A comparison of the exobase approximation to a Monte Carlo method. *??jnlIcarus* 204, 527–544. doi:10.1016/j.icarus.2009.07.005.
- Froese Fischer, C., Tachiev, G., 2004. Breit-Pauli energy levels, lifetimes, and transition probabilities for the beryllium-like to neon-like sequences. *Atomic Data and Nuclear Data Tables* 87, 1–184. doi:10.1016/j.adt.2004.02.001.
- Gao, H., Ng, C.Y., 2019. Quantum state-to-state vacuum ultraviolet photodissociation dynamics of small molecules. *Chinese Journal of Chemical Physics* 32, 23–34. doi:10.1063/1674-0068/cjcp1812290.
- Gérard, J.C., Aoki, S., Willame, Y., Gkouvelis, L., Depiesse, C., Thomas, I.R., Ristic, B., Vandaele, A.C., Daerden, F., Hubert, B., Mason, J., Patel, M.R., López-Moreno, J.J., Bellucci, G., López-Valverde, M.A., Beeckman, B., 2020. Detection of green line emission in the dayside atmosphere of Mars from NOMAD-TGO observations. *??jnlNature* 124, 5–8. doi:10.1029/2019JA026596.
- Gkouvelis, L., Gérard, J.C., Ritter, B., Hubert, B., Schneider, N.M., Jain, S.K., 2018. The O(¹S) 297.2 nm Dayglow Emission: A Tracer of CO₂ Density Variations in the Martian Lower Thermosphere. *Journal of Geophysical Research (Planets)* 123, 3119–3132. doi:10.1029/2018JE005709.
- Gkouvelis, L., Gérard, J.C., Ritter, B., Hubert, B., Schneider, N.M., Jain, S.K., 2020. Airglow remote sensing of the seasonal variation of the Martian upper atmosphere: MAVEN limb observations and model comparison. *??jnlIcarus* 341, 113666. doi:10.1016/j.icarus.2020.113666.
- Gronoff, G., Wedlund, C.S., Mertens, C.J., Barthélemy, M., Lillis, R.J., Witasse, O., 2012a. Computing uncertainties in ionosphere-airglow models: II. The Martian airglow. *Journal of Geophysical Research (Space Physics)* 117, A05309. doi:10.1029/2011JA017308.
- Gronoff, G., Wedlund, C.S., Mertens, C.J., Lillis, R.J., 2012b. Computing uncertainties in ionosphere-airglow models: I. Electron flux and species production uncertainties for Mars. *Journal of Geophysical Research (Space Physics)* 117, A04306. doi:10.1029/2011JA016930.
- Guberman, S.L., 1988. The production of O(¹D) from dissociative recombination of O₂⁺. *??jnlPlanet. Space Sci.*, 47–53doi:10.1016/0032-0633(88)90145-6.
- Huestis, D.L., Slanger, T.G., 2006. DPS. American Astronomical Society 38, 62.20.
- Huestis, D.L., Slanger, T.G., Sharpee, B.D., Fox, J.L., 2010. Chemical origins of the Mars ultraviolet dayglow. *Faraday Discuss.* 147, 307. doi:10.1039/c003456h.
- Jain, S.K., 2013. Dayglow emissions on Mars and Venus, Phd. Thesis. Ph.D. thesis. Cochin University of Science and Technology, India. India. URL: <https://dyuthi.cusat.ac.in/jspui/handle/purl/3688>.
- Jain, S.K., Bhardwaj, A., 2012. Impact of solar EUV flux on CO Cameron band and CO₂ UV doublet emissions in the dayglow of Mars. *??jnlPlanet. Space Sci.* 64, 110 – 122.
- Jain, S.K., Stewart, A.I.F., Schneider, N.M., Deighan, J., Stiepen, A., Evans, J.S., Stevens, M.H., Chaffin, M.S., Crismani, M., McClintock, W.E., Clarke, J.T., Holsclaw, G.M., Lo, D.Y., Lefèvre, F., Montmessin, F., Thiemann, E.M.B., Eparvier, F., Jakosky, B.M., 2015. The structure and variability of Mars upper atmosphere as seen in MAVEN/IUVS dayglow observations. *??jnlGeophys. Res. Lett.* 42, 9023–9030. doi:10.1002/2015GL065419.
- Krauss, M., Neumann, D., 1975. On the interaction of O(¹S) with O(³P). *Chemical Physics Letters* 36, 372–374. doi:10.1016/0009-2614(75)80259-4.
- Leblanc, F., Chaufray, J.Y., Lilensten, J., Witasse, O., Bertaux, J.L., 2006. Martian dayglow as seen by the SPICAM UV spectrograph on Mars Express. *Journal of Geophysical Research (Planets)* 111, E09S11. doi:10.1029/2005JE002664.
- Lu, Z., Chang, Y.C., Benitez, Y., Luo, Z., Houria, A.B., Ayari, T., Al-Mogren, M.M., Hochlaf, M., Jackson, W.M., Ng, C.Y., 2015. State-to-state vacuum ultraviolet photodissociation study of CO₂ on the formation of state-correlated CO(X¹Σ⁺; v) with O(¹D) and O(¹S) photoproducts at 11.95–12.22 eV. *Physical Chemistry Chemical Physics (Incorporating Faraday Transactions)* 17, 11752–11762. doi:10.1039/C5CP01321F.
- Núñez-Reyes, D., Hickson, K.M., 2018. Kinetics of the Gas-Phase O(¹D) + CO₂ and C(¹D) + CO₂ Reactions over the 50–296 K range. *Journal of Physical Chemistry A* 122, 4002–4008. doi:10.1021/acs.jpca.8b01964.
- Raghuram, S., Bhardwaj, A., 2012. Model for the production of CO Cameron band emission in Comet 1P/Halley. *??jnlPlanet. Space Sci.* 63, 139–149. doi:10.1016/j.pss.2011.11.011, arXiv:1201.6291.
- Raghuram, S., Bhardwaj, A., 2020. CO+ first-negative band emission: A tracer for CO in the Martian upper atmosphere. *??jnlA&A* 639, A60. doi:10.1051/0004-6361/202038147.
- Raghuram, S., Hutsemékers, D., Opitom, C., Jehin, E., Bhardwaj, A., Manfroid, J., 2020. Forbidden atomic carbon, nitrogen, and oxygen emission lines in the water-poor comet C/2016 R2 (Pan-STARRS). *??jnlA&A* 635, A108. doi:10.1051/0004-6361/201936713, arXiv:2001.03315.
- Rosén, S., Peverall, R., Larsson, M., Le Padellec, A., Semaniak, J., Larson, Å., Strömholm, C., van der Zande, W.J., Danared, H., Dunn, G.H., 1998. Absolute cross sections and final-state distributions for dissociative recombination and excitation of CO⁺(v=0) using an ion storage ring. *??jnlPhys. Rev. A* 57, 4462–4471. doi:10.1103/PhysRevA.57.4462.
- Schofield, K., 1978. Rate constants for the gaseous interaction of O(²D₂) and O(²S₀) - a critical evaluation. *Journal of Photochemistry* 9, 55 – 68. doi:10.1016/0047-2670(78)87006-3.
- Simon, C., Witasse, O., Leblanc, F., Gronoff, G., Bertaux, J.L., 2009.

- Dayglow on Mars: Kinetic modelling with SPICAM UV limb data. *Planet. Space Sci.* 57, 1008–1021. doi:10.1016/j.pss.2008.08.012.
- Song, Y., Gao, H., Chang, Y.C., Lu, Z., Ng, C.Y., Jackson, W.M., 2014. Photodissociation of CO₂ between 13.540 eV and 13.678 eV. *Physical Chemistry Chemical Physics (Incorporating Faraday Transactions)* 16, 563. doi:10.1039/C3CP53250J.
- Stewart, A.I., 1972. Mariner 6 and 7 Ultraviolet Spectrometer Experiment: Implications of CO₂⁺, CO and O Airglow. *J. Geophys. Res.* 77, 54. doi:10.1029/JA077i001p00054.
- Streit, G.E., Howard, C.J., Schmeltekopf, A.L., Davidson, J.A., Schiff, H.I., 1976. Temperature dependence of O(¹D) rate constants for reactions with O₂, N₂, CO₂, O₃, and H₂O. *J. Chem. Phys.* 65, 4761–4764. doi:10.1063/1.432930.
- Sutradhar, S., Samanta, B.R., Samanta, A.K., Reisler, H., 2017. Temperature dependence of the photodissociation of CO₂ from high vibrational levels: 205–230 nm imaging studies of CO(X¹Σ⁺) and O(³P, ¹D) products. *J. Chem. Phys.* 147, 013916. doi:10.1063/1.4979952.
- Thiemann, E.M.B., Chamberlin, P.C., Eparvier, F.G., Templeman, B., Woods, T.N., Bougher, S.W., Jakosky, B.M., 2017. The MAVEN EUVM model of solar spectral irradiance variability at Mars: Algorithms and results. *Journal of Geophysical Research (Space Physics)* 122, 2748–2767. doi:10.1002/2016JA023512.
- Viggiano, A.A., Ehlerding, A., Hellberg, F., Thomas, R.D., Zhaunerchyk, V., Geppert, W.D., Montaigne, H., Larsson, M., Kaminska, M., Österdahl, F., 2005. Rate constants and branching ratios for the dissociative recombination of CO₂⁺. *J. Chem. Phys.* 122, 226101–226101. doi:10.1063/1.1926283.
- Wiese, W.L., Fuhr, J.R., Deters, T.M., 1996. Atomic transition probabilities of carbon, nitrogen, and oxygen: A critical data compilation. *Am. Chem. Soc., Washington, D. C.*
- Yee, J.H., Guberman, S.L., Dalgarno, A., 1990. Collisional quenching of O(¹D) by O(³P). *Planet. Space Sci.* 38, 647–652. doi:10.1016/0032-0633(90)90071-W.